Anal. Chem. **2006,** *78,* 3800−3806

Probing Interfacial Chemistry of Single Droplets with Field-Induced Droplet Ionization Mass Spectrometry: Physical Adsorption of Polycyclic Aromatic Hydrocarbons and Ozonolysis of Oleic Acid and Related Compounds

Ronald L. Grimm, Robert Hodyss, and J. L. Beauchamp*

Division of Chemistry and Chemical Engineering and the Beckman Institute, California Institute of Technology, Pasadena, California 91125

The recently developed technique of field-induced droplet ionization (FIDI) is applied to study interfacial chemistry of a single droplet. In a new variation of the FIDI method, 1−2-mm-diameter droplets hang from a capillary and undergo heterogeneous reactions between solution-phase analytes and gas-phase species. Following a specified reaction time, the application of a high electric field induces FIDI in the droplet, generating fine jets of highly charged progeny droplets that are characterized by mass spectrometry. Sampling over a range of delay times following exposure of the droplet to gas-phase reactants, the spectra yield the temporal variation of reactant and product concentrations. We illustrate the technique with three examples: the adsorption of the polycyclic aromatic hydrocarbon naphthalene into a water−methanol droplet, the ozonolysis of oleic acid, and localization of the carbon−carbon double bond within a lysophosphatidic acid. Gas-phase naphthalene reacts with 80% methanol−20% water droplets containing 100 μM silver nitrate. Positive ion mass spectra show increasing concentrations of silver ion−naphthalene adducts as exposure times increase. To examine the ozonolysis of organic molecules, gas-phase ozone generated by a mercury pencil-style lamp reacts with either 10 μM oleic acid or 100 μM oleoyl-L-α-lysophosphatidic acid (LPA; 18:1). Negative ion spectra from the ozonolysis of oleic acid show azelaic acid and 9-oxononanoic acid as the principle reaction products. Ozonolysis products from LPA (18:1) unambiguously demonstrate the double bond position in the original phosopholipid.

Chemistry on and within liquid droplets is ubiquitious in nature and anthropomorphic processes, yet we have only begun to understand and harness such reactions. Liu and Dasgupta reviewed applications of liquid droplets to problems including windowless spectroscopy, solvent extraction, and trace gas detection.[1] Because of the desire to understand the behavior of aerosols in the atmosphere, much of the recent work is devoted to understanding heterogeneous reactions between droplets and reactive gas-phase species.[2] Popular techniques for studying atmospherically relevant heterogeneous chemistry include falling-drop and aerosol time-of-flight mass spectrometry (MS) experiments. Real-time Raman spectroscopy has enabled researchers to examine heterogeneous reactions on single droplets suspended in an electrodynamic balance.[3−6] The Agnes group established the viability of offline mass spectrometric analysis of individual soft-landed droplets that had previously been suspended in an electrodynamic balance. They further demonstrated that the suspended droplet may undergo heterogeneous reactions that may be subsequently characterized through offline mass spectrometry.[7,8]

To that end, single droplet mass spectrometry represents an ideal solution to the challenges presented by the analysis of microliters and less of sample and the online characterization of heterogeneous and interfacial reaction chemistry occurring on individual droplets. Recently our laboratory pioneered field-induced droplet ionization mass spectrometry (FIDI-MS).[9] In a critically high electric field, E_c^0, given by eq 1, neutral droplets

$$E_c^{\,0} \approx (5.28\sigma/8\pi\epsilon_0 r)^{1/2} \qquad (1)$$

elongate parallel to the field, developing two opposing conical tips that emit jets of oppositely charged progeny droplets.[10−12]

* To whom correspondence should be addressed. E-mail: jlbchamp@caltech.edu.

(1) Liu, H. H.; Dasgupta, P. K. *Microchem. J.* **1997**, *57*, 127−136.
(2) Finlayson-Pitts, B. J.; Pitts, J. N., Jr. *Chemistry of the Upper and Lower Atmosphere: Theory, Experiments, and Applications*; Academic Press: San Diego, 2000.
(3) Davis, E. J.; Aardahl, C. L.; Widmann, J. F. *J. Dispersion Sci. Technol.* **1998**, *19*, 293−309.
(4) Buehler, M. F.; Davis, E. J. *Colloids Surf., A* **1993**, *79*, 137−149.
(5) Musick, J.; Popp, J. *Phys. Chem. Chem. Phys.* **1999**, *1*, 5497−5502.
(6) Musick, J.; Popp, J.; Trunk, M.; Kiefer, W. *Appl. Spectrosc.* **1998**, *52*, 692−701.
(7) Bogan, M. J.; Agnes, G. R. *Anal. Chem.* **2002**, *74*, 489−496.
(8) Feng, X.; Bogan, M. J.; Chuah, E.; Agnes, G. R. *J. Aerosol Sci.* **2001**, *32*, 1147−1159.
(9) Grimm, R. L.; Beauchamp, J. L. *J. Phys. Chem. B* **2003**, *107*, 14161−14163.
(10) Macky, W. A. *Proc. R. Soc. A* **1931**, *133*, 565−586.
(11) Taylor, G. *Proc. R. Soc. London, Ser. A* **1964**, *280*, 383−397.
(12) Basaran, O. A.; Scriven, L. E. *Phys. Fluids A* **1989**, *1*, 799−809.

10.1021/ac0601922 CCC: $33.50
Published on Web 04/21/2006

This critical field is known as the Taylor limit, named for G. I. Taylor, where ϵ_0 is the permittivity of free space while r and σ are the droplet radius and surface tension, respectively. Using a constant stream of droplets generated by a vibrating orifice aerosol generator, we demonstrated that the charged progeny droplets emitted from parent droplets in a FIDI event are a viable source of gas-phase ions for mass analysis.[9] Rapidly switched electric fields and synchronized visualization allowed us to characterize the dynamics of the FIDI process.[13] The time scale of droplet elongation, tip formation, and progeny droplet generation slightly above E_c^0 is related to the time scale of the natural harmonic oscillations slightly below E_c.[0] Equation 2 approximates the time scale for FIDI, τ_{FIDI}, and is a function of bulk solution parameters including the density, ρ.[13]

$$\tau_{FIDI} = 2.3(r^3\rho/\sigma)^{1/2} \quad (2)$$

Understanding the critical field and the time scale for FIDI enables new applications of mass spectrometric analyses to chemical reactions occurring in small droplets. From eqs 1 and 2, millimeter-sized droplets generally require $(1-2) \times 10^6$ V m^{-1} fields to initiate FIDI jetting and charged progeny formation on the millisecond time scale. Therefore, chemical reactions within and on the droplet that occur on longer time scales may be directly probed with a rapid high-voltage pulse, and the ejected progeny may be characterized by mass analysis. Such characterizations motivate the present investigation.

Herein, we demonstrate the viability of online analysis of chemical reactions within single droplets, formed on and hanging from a fine capillary, by FIDI-MS and apply the technique to three processes between reactive gas-phase molecules and analytes dissolved in liquid droplets. Complexation between the polycyclic aromatic hydrocarbon naphthalene and solution-phase silver ions demonstrates the adsorption of gas-phase organics into the droplet. Naphthalene ions do not traditionally appear in mass spectra from soft-ionization sources such as electrospray (ESI) and FIDI. However, naphthalene forms strong cation$-\pi$ complexes with metal ions that are preserved by soft-ionization techniques. Silver ions from dissolved silver nitrate are employed because of the characteristic isotope pattern at 107 and 109 m/z in nearly equal ratio.

We separately consider the reactions of gas-phase ozone with oleic acid and oleoyl-L-α-lysophosphatidic acid (LPA; 18:1). Researchers consider the reaction of gas-phase ozone with oleic acid as a model system for heterogeneous reaction chemistry, with significant implications for atmospheric chemistry.[14−19] Cooking involving animal and vegetable oils is a significant source of atmospheric oleic acid, and environmental field measurements suggest oleic acid is present in nanogram per cubic meter concentrations in urban areas with a lifetime on the order of days.[20,21] Ziemann presented a rigorous mechanism of pure oleic acid ozonolysis.[22] Scheme 1 details a simplified version of this mechanism showing the important intermediates and expected reaction products. Briefly, ozone adds across the oleic acid (**1**) double bond forming a primary ozonide (**2**). This energetic ozonide dissociates either into Crigee intermediate **3′** and nonanal (**4**) or into 9-oxononanoic acid (**5**) and intermediate **6′**. These excited intermediates may isomerize into azelaic acid (**3**) or nonanoic acid (**6**), respectively. Alternatively, the intermediates may recombine with their respective aldehydes to form a secondary ozonide **7**, which will also dissociate to give products **3**−**6**.[2,14,22,23] The presence of an inert solvent and the absence of

Scheme 1. Oxidation of Oleic Acid (1) by Ozone on Surfaces Proceeding through the Dissociation of the Primary Ozonide 2 Either into Crigee Intermediate 3′ and Nonanal (4) or into Intermediate 6′ and 9-Oxononanoic Acid (5)[a]

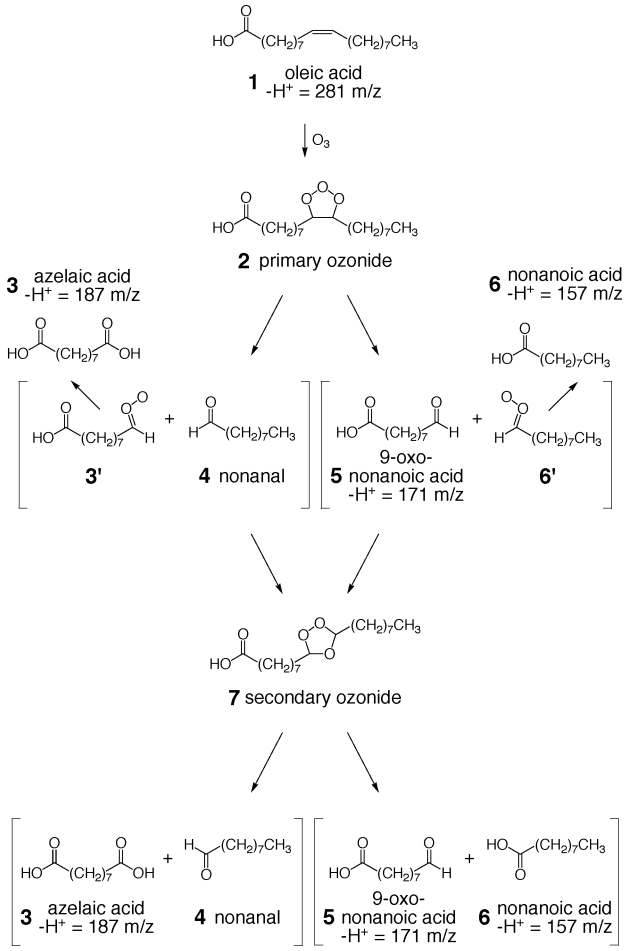

[a] The energetic intermediates may isomerize to form azelaic acid (**3**) or nonanoic acid (**6**), respectively. Alternatively, the intermediates may be stabilized and recombine to form the secondary ozonide **7**, which will also dissociate into (**3**)−(**6**).

(13) Grimm, R. L.; Beauchamp, J. L. *J. Phys. Chem. B* **2005**, *109*, 8244−8250.
(14) Hung, H. M.; Katrib, Y.; Martin, S. T. *J. Phys. Chem. A* **2005**, *109*, 4517−4530.
(15) Knopf, D. A.; Anthony, L. M.; Bertram, A. K. *J. Phys. Chem. A* **2005**, *109*, 5579−5589.
(16) Katrib, Y.; Martin, S. T.; Hung, H. M.; Rudich, Y.; Zhang, H. Z.; Slowik, J. G.; Davidovits, P.; Jayne, J. T.; Worsnop, D. R. *J. Phys. Chem. A* **2004**, *108*, 6686−6695.
(17) Smith, G. D.; Woods, E.; DeForest, C. L.; Baer, T.; Miller, R. E. *J. Phys. Chem. A* **2002**, *106*, 8085−8095.
(18) Moise, T.; Rudich, Y. *J. Phys. Chem. A* **2002**, *106*, 6469−6476.
(19) Hearn, J. D.; Smith, G. D. *J. Phys. Chem. A* **2004**, *108*, 10019−10029.
(20) Rogge, W. F.; Hildemann, L. M.; Mazurek, M. A.; Cass, G. R.; Simonelt, B. R. T. *Environ. Sci. Technol.* **1991**, *25*, 1112−1125.
(21) Morris, J. W.; Davidovits, P.; Jayne, J. T.; Jimenez, J. L.; Shi, Q.; Kolb, C. E.; Worsnop, D. R.; Barney, W. S.; Cass, G. *Geophys. Res. Lett.* **2002**, *29*, art. no. 1357.
(22) Ziemann, P. J. *Faraday Discuss.* **2005**, *139*, 469−490.

further reactive species minimize other products formed though reactions involving the Crigee intermediates.[2] The micromolar concentrations of oleic acid employed our experiments allow for this simplification. The short (~10 nm) characteristic diffusion distance of ozone into pure oleic acid supports the model of a heterogeneous reaction at the air−droplet interface.[17,18] This reaction is well-studied, but questions remain regarding the partitioning of products and the relative yields from the ozonolysis in Scheme 1.[14] Katrib and co-workers summarized recent experiments that suggest nonanal partitions into the vapor phase and would not be detected by FIDI-MS of the droplet. They found the formation of 9-oxononanoic acid dominates the products relative to only small quantities of nonanoic acid and azelaic acid.[16]

Because ozone preferentially attacks organic molecules at carbon−carbon double bonds with few rearrangements, ozonolysis products have a predictable mass based on the reaction shown in Scheme 1. Therefore, the product ion mass may be employed to localize the position of a double bond within a reactant organic molecule. For example, Privett and Nickell demonstrated double bond localization by ozonolysis with subsequent product analysis by gas chromatography.[24] Ozonolysis is one of many chemical derivatization techniques including hydrazine reduction,[25] silylation,[26] and epoxidaion[27] that react to break the double bond but maintain the remaining structural information. Early high-resolution MS studies characterize the reaction of olefins with Ti^+ [28] and Co^+.[29] Peake and Gross applied similar reaction chemistry to localize double bonds in large olefins using Fe^+ [30,31] and Cu^+.[32]

In general, double bond determination by ozonolysis requires separate reaction and characterization steps that may be simplified using online FIDI-MS or ESI-MS. Thomas and co-workers recently demonstrated ozonolysis of phospholipids directly within an electrospray ionization plume.[33] We demonstrate the viability of online FIDI-MS for double bond localization with the reaction between ozone and LPA (18:1). Scheme 2 shows LPA (18:1) (**8**), and the expected aldehyde **9** and acid **10**, reaction products based on the known oleic acid reaction with ozone. Additionally, the Crigee intermediate may react with methanol forming an α-methoxyhydroperoxide (**11**).[34]

EXPERIMENTAL SECTION

Online FIDI-MS Technique. Figure 1 shows a cartoon of the droplet formation, gas-phase exposure, and FIDI-MS sequence. Initially, a 28-gauge stainless steel capillary (355-μm o.d., 178-μm i.d.; Small Parts Inc.) feeds an analyte-containing solution to establish a 1−2-mm droplet (frame A). The liquid surface tension suspends the droplet on the capillary between the atmospheric sampling inlet of a ThermoFinnigan LCQ Deca mass spectrometer and a parallel plate electrode. The parallel plate electrode and the MS sampling inlet are separated by 6 mm and are bisected by

Scheme 2. Expected Products in the Ozonolysis of LPA (18:1) (8)[a]

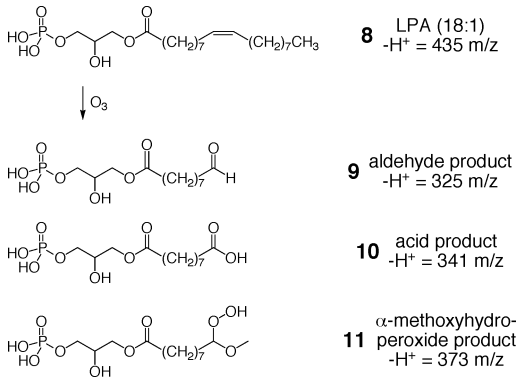

[a] These are the aldehyde reaction product **9**, the acid reaction product **10**, and the α-methoxyhydroperoxide product **11**.

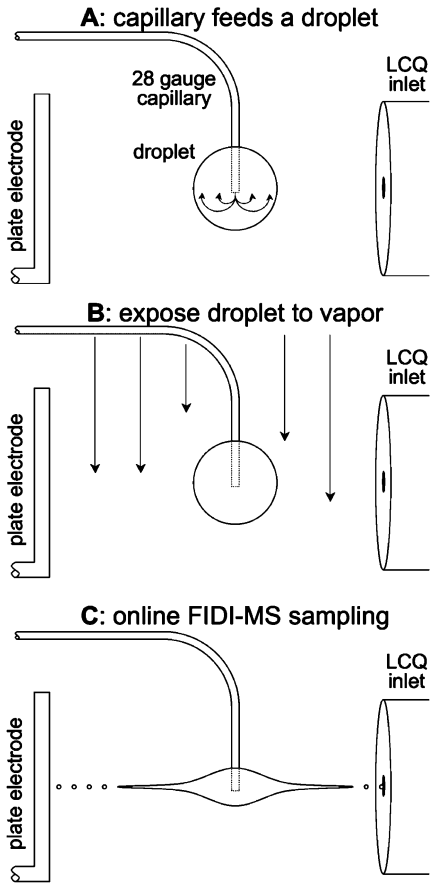

Figure 1. Cartoon depiction of the online FIDI-MS process. A capillary feeds analyte-containing solution forming a droplet suspended from the end of that capillary (A). All electrical components remain at ground as the droplet grows and reacts in a field-free environment. Gas-phase reactants such as aromatics or ozone flow over the droplet resulting in heterogeneous reactions between the gas-phase and solution-phase species (B). After a suitable period of exposure to the vapor-phase species, a high-voltage pulse on the plate electrode initiates the FIDI process (C). The charged jets enter the atmospheric sampling inlet of the LCQ for mass analysis.

(23) Wadia, Y.; Tobias, D. J.; Stafford, R.; Finlayson-Pitts, B. J. *Langmuir* **2000**, *16*, 9321−9330.
(24) Privett, O. S.; Nickell, E. C. *Lipids* **1966**, *1*, 98−103.
(25) Roehm, J. N.; Privett, O. S. *J. Lipid Res.* **1969**, *10*, 245-&.
(26) Ariga, T.; Araki, E.; Murata, T. *Anal. Biochem.* **1977**, *83*, 474−483.
(27) Tumlinson, J. H.; Heath, R. P.; Doolittle, R. E. *Anal. Chem.* **1974**, *46*, 1309−1312.
(28) Allison, J.; Ridge, D. P. *J. Am. Chem. Soc.* **1977**, *99*, 35−39.
(29) Armentrout, P. B.; Halle, L. F.; Beauchamp, J. L. *J. Am. Chem. Soc.* **1981**, *103*, 6624−6628.
(30) Peake, D. A.; Gross, M. L.; Ridge, D. P. *J. Am. Chem. Soc.* **1984**, *106*, 4307−4316.
(31) Peake, D. A.; Gross, M. L. *Anal. Chem.* **1985**, *57*, 115−120.
(32) Peake, D. A.; Gross, M. L. *J. Am. Chem. Soc.* **1987**, *109*, 600−602.
(33) Thomas, M. C.; Mitchell, T. W.; Blanksby, S. J. *J. Am. Chem. Soc.* **2006**, *128*, 58−59.
(34) Gbara-Haj-Yahia, I.; Zvilichovsky, G.; Seri, N. *J. Org. Chem.* **2004**, *69*, 4135−4139.

the droplet. During droplet formation and reaction, the inlet, electrode, and capillary remain electrically grounded, allowing reactions to proceed in a field-free environment. Heterogeneous reactions ensue with continuous vapor exposure (frame B). Reactions occur for a user-specified reaction time between 0 and 60 s before a high-voltage pulse on the electrode applies a strong electric field to the droplet resulting in the ejection of jets of small, highly charged progeny droplets (frame C).

Previous studies on 225-μm methanol droplets required custom-made solid-state MOSFET switching circuitry to achieve submicrosecond switching.[13] In the present investigation, the millimeter-sized droplets require millisecond fields applied by commercial high-voltage reed relays (W102HVX-3, and W102VX-50, Magnecraft, Northfield, IL) and modest timing circuitry. The high-voltage pulse establishes a 1.5×10^6 V m^{-1}, ~5-ms field to achieve jetting and FIDI as required by eqs 1 and 2. To remain field-neutral, the capillary voltage pulses to half the voltage applied to the plate electrode. When pulsed, typical voltages are 8−10 kV for the plate electrode, 4−5 kV for the capillary, and 0 V for the LCQ sampling inlet. A positive high-voltage pulse directs positively charged progeny into the mass spectrometer for positive ion mass analysis and negative high voltage results in negative ion mass spectra. After FIDI-MS, flowing additional solution through the tubing causes the existing droplet to fall off and forms a fresh droplet for reaction.

Because the FIDI source directs ions into the LCQ sampling inlet, the traditional electrospray source is removed. All components employed are mounted on a removable sled that rests on the track for the electrospray source. Independent three-dimensional stages control the position of the plate electrode and capillary wire to allow proper alignment of the droplet with the sampling inlet of the mass spectrometer. With the aid of a small mirror, a CCD camera monitors the FIDI region and droplet throughout the process. Figure 2 shows a schematic of the FIDI-MS setup (frame A) and CCD images of a single droplet undergoing FIDI (frames B and C). Even though the FIDI process samples a small fraction of the total droplet volume, the droplet is replaced after each sampling event because of the mixing associated with post-FIDI droplet relaxation.

Reaction Conditions. For the reaction between naphthalene and silver ions, naphthalene-saturated air at 353 K (99%, Sigma, 0.87 Torr partial pressure[35]) continually flows through the FIDI region at 500 mL min^{-1}. A solution of 100 μM silver nitrate (ACS reagent, 99.9+%, Alfa Aesar) in 20% water and 80% methanol is used to form the droplets. Simultaneously, a +9.0-kV, 6-ms pulse on the plate electrode and a +4.5-kV, 6-ms pulse on the capillary establishes a 1.5×10^6 V m^{-1} field that initiates FIDI following reaction times between 0 and 30 s. Positively charged progeny droplets are directed into the LCQ, which is set to positive ion mode.

For the ozonolysis reactions, a pencil-style UV calibration lamp (model 6035, Oriel) generates ~75 ppb ozone in air that continually washes through the FIDI region at 500 mL min^{-1}. Either 10 μM oleic acid (>99.0%, Fluka) or 100 μM LPA (18:1; sodium salt, 98%, Sigma) solutions in 90% dimethyl formamide (DMF) and 10% methanol feed the droplet source. DMF is employed because it has low vapor pressure and an evaporation rate similar to water. However, because $E_{FIDI} \propto \sigma^{1/2}$, the comparatively low surface tension of DMF allows more modest fields than required for water droplets of the same size. The low vapor pressure and slow evaporation rate results in a negligible size decrease over the maximum 60-s time scale of the ozonolysis experiments. The −9.2- and −4.6-kV, 6-ms pulses to the plate electrode and capillary initiate FIDI and direct negatively charged progeny into the LCQ for negative ion mass analysis.

To confirm peak assignments in the FIDI-MS spectra, commercially acquired samples of the expected ozonolysis reaction products are electrosprayed into the LCQ. Peaks in the FIDI-MS and ESI-MS spectra are compared as well as the peak distributions from collision-induced dissociation (CID) spectra. Nonanoic acid (>99.5%, Fluka), azelaic acid (>99.0%, Fluka), and 9-oxononanoic acid (5 mg in ethanol, Indofine Chemicals) are used without further purification. Tunable LCQ instrument parameters remain identical for both the FIDI and electrospray experiments.

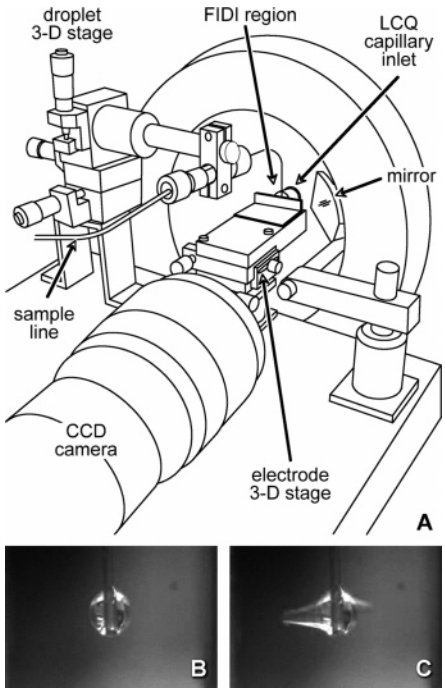

Figure 2. Schematic of the single droplet FIDI-MS apparatus (A) and images of 2-mm-diameter droplets in a field-free environment (B) and undergoing FIDI (C). A droplet is mechanically suspended in the high field FIDI region defined by a parallel plate electrode and the LCQ sampling inlet. Independent three-dimensional translation stages align the droplet and the electrode. A CCD camera visualizes the FIDI region reflected in a small mirror, and the droplet is oriented such that the charged progeny jets are directed into the MS capillary for mass analysis. CCD camera images shown in (B) and (C) provide information regarding droplet size and alignment with the LCQ inlet.

RESULTS AND DISCUSSION

Naphthalene and Silver Ions. Figure 3 shows the positive ion spectrum for (A) <1-, (B) 10-, and (C) 30-s exposures to naphthalene before being sampled by FIDI-MS. The instantaneous positive ion FIDI-MS spectrum (Figure 3A) shows silver ion−solvent complexes $Ag^+(H_2O)(MeOH)$ and $Ag^+(MeOH)_2$ at 157, 159 and 171, 173 m/z, respectively. This spectrum is

(35) Yaws, C. L. *Chemical Properties Handbook: Physical, Thermodynamic, Environmental, Transport, Safety, And Health Related Properties for Organic and Inorganic Chemicals*; McGraw-Hill: New York, 1999.

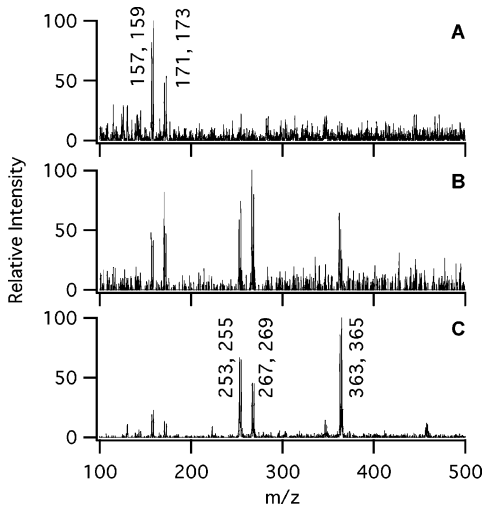

Figure 3. Association of gas-phase naphthalene with solution-phase silver ions. When the droplet undergoes FIDI-MS immediately following formation (frame A), $Ag^+(H_2O)(MeOH)$ complexes at 157 and 159 *m*/*z* and $Ag^+(MeOH)_2$ complexes at 171 and 173 *m*/*z* dominate the spectrum. Following a 10-s exposure to naphthalene vapor (frame B), spectra show a distribution of the reactant clusters as well as naphthalene monomer adducts at 253 and 255 *m*/*z* due to $Ag^+(H_2O)$-(naphthalene) and at 267 and 269 *m*/*z* due to $Ag^+(MeOH)$-(naphthalene). Frame B also shows the formation of a naphthalene dimer−silver cation complex at 363 and 365 *m*/*z*. After a 30-s exposure (frame C), the dimer complex dominates the spectrum.

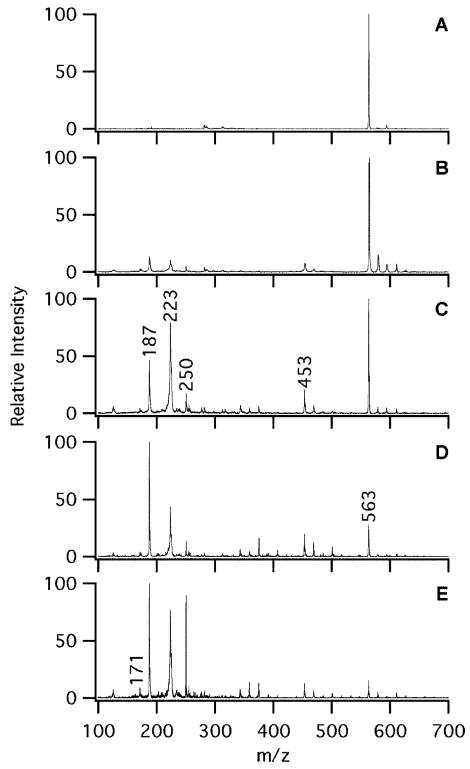

Figure 4. Oxidation of oleic acid by ozone as a function of time. In the absence of ozone, the negative ion FIDI-MS spectrum of oleic acid is dominated by the singly deprotonated dimer peak at 563 *m*/*z*. Successive frames show reaction with (B) <1-, (C) 5-, (D) 20-, and (E) 60-s exposures. Oxidation products are dominated by deprotonated azelaic acid at 187 *m*/*z*, doubly hydrated deprotonated azelaic acid at 223 *m*/*z*, an unknown cluster containing azelaic acid at 250 *m*/*z*, and a deprotonated oleic acid/azelaic acid cluster at 453 *m*/*z*.

characteristic of the ESI-MS spectrum of the same liquid sample and indicates negligible complexation to naphthalene when the silver ion-containing droplets undergo FIDI immediately following droplet formation. After a 3-s exposure, peaks at 253, 255 and 267, 269 m/z appear, which we attribute to $Ag^+(H_2O)$(naphthalene) and Ag^+(MeOH)(naphthalene) complexes. When allowed to react for 30 s, spectra are dominated by a naphthalene dimer complex $Ag^+(naphthalene)_2$ at 363, 365 m/z with lower concentrations of the monomer complexes and the original reactant silver ion species.

Ozonolysis of Oleic Acid. Figure 4 shows the negative ion FIDI-MS spectra for the ozonolysis of oleic acid. The singly deprotonated dimer at 563 m/z dominates the FIDI-MS spectrum of oleic acid in the absence of ozone (frame A) as well as the electrospray spectrum of the same solution (not shown). Frames B−E show increasing relative concentrations of the products to reactants (563 m/z) after instantaneous (<1 s), 5-, 20-, and 60-s exposures to ozone, respectively. Principle reaction products include deprotonated azelaic acid (**3**), at 187 m/z, and cluster ion peaks containing azelaic acid at 223 and 250 m/z (discussed later). CID reactions of the 187 m/z ion are identical to CID electrospray mass spectra from the commercially supplied azelaic acid. The 9-oxononanoic acid (**5**) is principally observed as a singly deprotonated complex with oleic acid at 453 m/z. CID of the 453 m/z ion yields both the 171 and 281 m/z ions characteristic of deprotonated 9-oxononanoic acid and oleic acid, respectively. After 60 s, spectra show a small quantity of deprotonated 9-oxononanoic acid at 171 m/z. Deprotonated nonanoic acid (**6**) is not observed as expected at 157 m/z in any of the spectra.

Low-energy CID spectra of the 223 and 250 m/z ions principally produce singly deprotonated azelaic acid indicating cluster parent ions. We attribute the peak at 223 m/z to a deprotonated cluster of azelaic acid and two water molecules. CID of the 223 m/z peak reveals azelaic acid at 187 m/z but virtually no signal at 205 m/z, which would correspond to a deprotonated cluster of azelaic acid and one water molecule. This behavior is also observed in the electrospray spectrum of azelaic acid in DMF with 0.1% water. Although water is not a principal component of the reactant solution, density functional theory calculations performed with CaCHe indicate exceptionally strong binding in doubly hydrated, deprotonated azelaic acid. We propose a ring complex in which doubly deprotonated azelaic acid forms four hydrogen bonds to the outer protons of the proton-bound water dimer in a Zundel-like water cluster. The stability of this cluster and the soft-ionization process characteristic of FIDI suggest that the deprotonated azelaic acid may complex to trace water impurities in the original solution or water within the mass spectrometer ion trap. This complex will be the subject of future reports. CID of the 250 m/z peak reveals azelaic acid at 187 m/z. This peak may be due to a deprotonated cluster of azelaic acid and nitric acid (63 Da); however, the ESI-MS of azelaic acid in DMF with 0.1% nitric acid did not reveal this cluster.

In general, the sum of the product ion peak intensities due to azelaic acid and its complexes is 5−25 times the sum of the overall intensity of peaks due to 9-oxononanoic acid and its clusters. However, relating product peak intensities to ozonolysis product yields requires an understanding of the overall relative ionization and detection efficiencies in the mass spectrometer. When electrosprayed into the mass spectrometer under otherwise

identical instrument parameters, a 10 μM equimolar mixture of 9-oxononanoic acid and azelaic acid shows a peak ratio of ~1:10. This indicates ozonolysis is producing roughly equal amounts of azelaic acid and 9-oxonanoic acid. This result contrasts with previous studies on pure oleic acid droplets that find more than a 5-fold excess of 9-oxonanoic acid over azelaic acid.[16,22] As discussed in the introduction, Scheme 1 presents a simplified mechanism that does not show additional ozonolysis products such as diperoxides and oligomers that give rise to additional sources of 9-oxonanoic acid.[22] These reaction pathways depend on the olefin concentration.[36] The low concentration of oleic acid in the present experiments minimizes these alternate pathways, which in turn maximizes the formation of the secondary ozonide **7** and products **3**−**6**. The roughly equal concentrations of azelaic acid and 9-oxonanoic acid produced in this study support the suppression of alternate reaction pathways and equal preference in the dissociation of the ozonides.

Interestingly, a 10 μM equimolar electrospray mass spectrum of nonanoic acid and 9-oxononanoic acid shows a peak ratio of ~2:3 yet no nonanoic acid is observed in the FIDI ozonolysis experiments. According to Scheme 1, formation of nonanoic acid is concurrent with formation of 9-oxononanoic acid. This indicates the ratio of nonanoic acid to 9-oxononanoic acid in the ozonolysis experiment should be similar to the intensity ratio in the equimolar electrospray. Peaks due to nonanal are not expected because negative ion soft-sampling produces poor signal from aldehydes and previous research shows nonanal partitioning into the vapor phase.[16,18]

This study considered ozone dissolved in 90% DMF/10% methanol because of the slow evaporation rate and low surface tension of this binary solvent system. However, this is not a solvent system directly relevant to atmospheric aerosols. Future studies are planned to quantify the reaction kinetics for this system and consider possible solvent effects in the ozonolysis of oleic acid sampled by FIDI-MS.

Localization of Carbon−Carbon Double Bonds. Based on the predicted pathways outlined and experimentally observed peaks supporting Scheme 1, the primary ozonolysis products are directly related to the structure of the original reactant. Figure 5A shows the negative ion FIDI-MS spectrum of LPA (18:1) in the absence of ozone. Primary peaks are due to deprotonated LPA (18:1) at 453 *m*/*z*, a deprotonated dimer at 871 *m*/*z*, a doubly deprotonated sodium-bound adduct at 893 *m*/*z*, and a deprotonated ester hydrolysis product at 153 *m*/*z*. Figure 5B shows the FIDI-MS spectrum for droplets exposed to ozone for 5 s. This reaction time was selected based on the oleic acid results, which showed significant amounts of both reactant and product ion signal after 5 s of ozone exposure (Figure 4C). Product ions include strong peaks at 325 and 373 *m*/*z* and a very weak signal at 341 *m*/*z* (magnified in the Figure 5B inset). The deprotonated reaction products at 325 and 341 *m*/*z* respectively correspond to the formation of an aldehyde and an organic acid at the ninth carbon atom in the ester in support of Scheme 2. This is indeed the location of the double bond in LPA (18:1), indicating that FIDI-MS successfully localizes double bonds and characterizes the reaction products with a soft-sampling ionization method. The peak

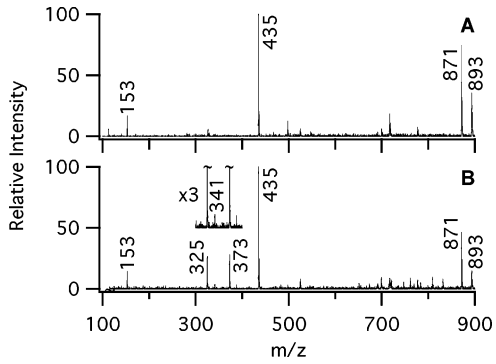

Figure 5. Oxidation of LPA (18:1) by ozone unambiguously demonstrates the location of the double bond along the hydrocarbon tail. In the absence of ozone (A), the singly deprotonated monomer at 435 *m*/*z*, the singly deprotonated dimer at 871 *m*/*z*, and the sodium-bound dianion peak at 893 *m*/*z* dominate the negative ion FIDI-MS spectrum of LPA (18:1). Frame B shows the FIDI-MS spectrum containing the reaction products following 5-s exposures to ozone including the aldehyde product peak at 325 *m*/*z* (**9**), a weak signal at 341 *m*/*z* from the acid product (**10**), and a peak at 373 *m*/*z* due to the Crigee intermediate reaction with methanol (**11**). Decomposition of the LPA ester bond results in the 153 *m*/*z* peak observed in all spectra.

at 373 *m*/*z* is likely an α-methoxyhydroperoxide species **11** formed by the reaction of the Crigee intermediate with a methanol solvent molecule. Thomas and co-workers observed similar species in the mass analysis of phospholipids oxidized within an electrospray ionization plume.[33] Considering the relative intensities of the 341 and 373 *m*/*z* ions, the α-methoxyhydroperoxide product likely constitutes the dominant reaction pathway of the Crigee intermediate in this experiment, resulting a low relative concentration of the acid **10**.

Heterogeneous Reactions at the Gas−Liquid Interface. Resistance models commonly explain chemistry between gas- and solution-phase species.[2] Such models break overall heterogeneous reactions into a series of steps such as gas diffusion to the droplet surface, surface accommodation and reaction, diffusion through the solution phase, and reactions in the solution. In developing these models, gas-phase reactants have a characteristic penetration distance within a droplet due to diffusion before reaction. This characteristic penetration distance, *l*, is commonly referred to as the *diffuso-reactive length* and is given by eq 3 for the penetration of ozone into an oleic acid-containing droplet.[17]

$$l = (D/k_2[\text{oleic acid}])^{1/2} \qquad (3)$$

In eq 3, D represents the diffusion constant of ozone in the liquid and is commonly approximated by 1.5×10^{-5} cm^2 s^{-1}, the diffusion constant of molecular oxygen in common organic solvents.[17] The initial concentration of oleic acid is 10 μM, and the bulk ozonolysis rate constant, $k_2 \sim 1 \times 10^6$ M^{-1} s^{-1}.[17] This predicts that ozone characteristically penetrates ~10 μm into the 1−2-mm droplets in this study. Reactions occur in the outer 1% of the droplet diameter, which supports the presence of interfacial chemistry. In the environment, only fine (<2.5-μm diameter, $PM_{2.5}$) and coarse (<10-μm diameter, PM_{10}) particulate matter have lifetimes long enough for reaction chemistry to occur. Therefore, at this concentration of oleic acid, the ozonolysis reactions would

(36) Bailey, P. S. *Ozonation In Organic Chemistry: Volume 1 Olefinic Compounds*; Academic Press: New York, 1978.

constitute bulk-phase processes within atmospherically relevant aerosol droplets.

CONCLUSIONS

Capillary-suspended 1−2-mm-diameter droplets undergo heterogeneous reactions between solution-phase analytes and gas-phase species. Reactions occur for a specified time before an applied strong electric induces FIDI and the production of charged progeny that are characterized by mass spectrometry. The technique is applied to three chemical systems. The adsorption of naphthalene into silver ion-containing droplets is demonstrated by the formation of silver ion−naphthalene adducts. Ozonolysis of droplets containing oleic acid produces 9-oxononanoic acid and azelaic acid in similar concentrations. Products from the ozonolysis of LPA (18:1) unambiguously demonstrate the double bond position in the original phosopholipid.

FIDI-MS allows for real-time monitoring of the reaction chemistry in single droplets. Such reactions may include environmental studies involving online characterization of the kinetics of heterogeneous reactions between gas-phase and solution-phase species and solution-phase photoinitiated reactions whose products are sampled by FIDI-MS after a predetermined reaction time. The applications may also be extended to include the examination of free falling droplets or those suspended in an electrodynamic balance or by acoustic levitation.

ACKNOWLEDGMENT

The authors thank Professors Richard Flagan and Barbara J. Finlayson-Pitts for their ongoing discussions and consideration. This material is based on work supported by the National Science Foundation under Grant CHE-0416381 and a grant from the Beckman Institute at Caltech.

Received for review January 28, 2006. Accepted March 23, 2006.

AC0601922